catalysts

MDPI

Article

Photocatalytic Oxidation of Methyl *Tert*-Butyl Ether in Presence of Various Phase Compositions of TiO_2

Marcel Šihor, Martin Reli *, Michal Vaštyl, Květoslava Hrádková, Lenka Matějová and Kamila Kočí

Institute of Environmental Technology, VŠB-Technical University of Ostrava, 17. listopadu 2172/15, 70800 Ostrava, Czech Republic; marcel.sihor@vsb.cz (M.Š.); michal.vastyl@vsb.cz (M.V.); kvetoslava.hradkova@vsb.cz (K.H.); lenka.matejova@vsb.cz (L.M.); kamila.koci@vsb.cz (K.K.)

* Correspondence: martin.reli@vsb.cz; Tel.: +420-597-327-304

Received: 21 November 2019; Accepted: 21 December 2019; Published: 26 December 2019

Abstract: MTBE (methyl *tert*-butyl ether) represents a rising threat to the environment, especially drinking water, and its effective removal (with all by-products) is necessary. Even a very low concentration of MTBE makes the water undrinkable; therefore, an effective treatment has to be developed. This work is focused on MTBE photocatalytic oxidation in presence of various TiO_2 photocatalysts with different phase composition prepared by different methods. It was confirmed the phase composition of TiO_2 had the most significant influence on the photocatalytic degradation of MTBE. The rutile phase more easily reduces adsorbed oxygen by photogenerated electrons to superoxide radical, supporting separation of charge carriers. The presence and concentrations of by-products have to be taken into account as well. The conversion of total organic carbon (TOC) was used for the comparison, 40% of TOC was removed after 1 h of irradiation in presence of TiO_2–ISOP–C/800 photocatalyst composed of anatase and rutile phase.

Keywords: photocatalysis; MTBE oxidation; TiO_2; anatase-rutile

1. Introduction

Environmental protection, especially water and air, is representing a serious challenge for current science. Transportation belongs among the pollution sources which negatively influence both air and water environment. The air pollution from transportation is well discussed, and there are various restrictions to decrease exhaust emissions as much as possible. However, the water pollution connected to transportation is not so apparent, especially to public knowledge. For example, methyl *tert*-butyl ether (MTBE), a gasoline additive, is a chemical compound used for increasing oxygen content in gasoline [1].

MTBE as fuel additive was used in 1979 for the first time. It was used to replace lead and as an octane enhancer [2]. The production of MTBE has increased ever since. The total consumption of MTBE reached 22.4 Mt annually in 2016, and this number is expected to increase to 26.5 Mt in 2021 [3]. Considering very high production levels of MTBE, it is expected to find this compound in the environment. Since the MTBE is rather easily dissolved in water, it is water sources where MTBE can be found. The problem is when drinking water is contaminated because even very low concentrations of MTBE can make drinking water undrinkable due to its offensive taste and odor. Since MTBE in drinking water has attracted attention quite recently, its harmful effects on human health after digestion are unclear [2]. However, higher concentrations of MTBE were reported to depress the nervous system, be genotoxic, irritate skin and eyes [1]. Water containing very low amount of MTBE, around 20 ppb and more, already smell like turpentine.

There are several ways how MTBE gets into the environment. Main sources of MTBE are accidental fuel leakages during transportation of storage containers and car accidents, but also unburned gasoline spilled from boats directly to surface waters [1]. As a result, MTBE is the second most commonly detected volatile organic compound in surface waters.

Currently, there are several methods for removing MTBE from water, for example, various adsorptions, air stripping, biodegradation, electrochemical oxidation, and advanced oxidation processes. All these methods are described and discussed in a review paper focused on technologies for removal of MTBE [1]. Advanced oxidation processes, especially photocatalysis proved to be a very promising method. It is the vision of very low costs for operating the technology that makes it so interesting. Photocatalysis found its way into basically all research fields during the last decade, and removal of MTBE is no exception. The photocatalytic decomposition of MTBE was studied using various semiconductor catalysts, which were modified or immobilized on the support, the catalysts were mostly based on TiO_2 [4–8] or ZnO [9–11].

This work is investigating the photocatalytic degradation of methyl *tert*-butyl ether in presence of various TiO_2 photocatalysts with different phase composition prepared by different methods.

2. Results and Discussion

The texture properties of TiO_2 photocatalysts prepared by various methods were evaluated using nitrogen physisorption (Table 1). The shape of the nitrogen adsorption/desorption isotherms of most of the photocatalysts can be categorized as IV type isotherms according the IUPAC classification [12], basically corresponding to the mesoporous materials. Based on the similarities of the shapes of isotherms, the TiO_2 photocatalysts may be divided to two groups of mesoporous materials; the first one includes TiO_2 photocatalysts prepared from titanium (IV) isopropoxide (TiO_2–ISOP–C/400, TiO_2–ISOP–PFC), the second one includes TiO_2 photocatalyst prepared from titanyl sulphate (TiO_2–TYS–C/450). TiO_2–ISOP–C/800 was not included in any of these two groups, since it is a nonporous material showing very low specific surface area (measured by Kr physisorption). The TiO_2–ISOP–C/400 and TiO_2–ISOP–PFC hysteresis loops were identified as the H2 type belonging to mesoporous adsorbents where the porous structure is complex and is not well-defined. It is evident the ISOP–based TiO_2 photocatalysts possess similarly smaller mesopores (pore width < 15 nm) (Figure 1b). However, TiO_2–ISOP–PFC shows significantly higher specific surface area and pore volume than TiO_2–ISOP–C/400 (Table 1), which may be attributed to the fact that TiO_2 nanocrystallites are less aggregated due to crystallization in pressurized fluids than under thermal treatment, and this different processing also results in different crystallinity of TiO_2–ISOP–PFC (i.e., bicrystalline anatase–brookite mixture). The TiO_2–TYS–C/450 hysteresis loop may be classified as the H3 type associated with aggregates of smaller TiO_2 nanocrystallites of broad crystallite size-distribution. Its porous structure comprises some macropores (Figure 1b). Concerning the effect of preparation parameters on TiO_2 textural properties, it is evident that the crystallization of ISOP–based TiO_2 in pressurized hot water and methanol led to lowered aggregation/sintration of TiO_2 crystallites reflected to enhanced specific surface area and well-developed porous structure of TiO_2 compared, e.g., to TiO_2–ISOP–C/400.

Table 1. Textural properties of investigated TiO_2 photocatalysts.

Photocatalyst Labeling	Physisorption		UV–Vis
	S_{BET} (m^2 g^{-1})	V_{ne} (cm^3_{liq} g^{-1})	Band Gap Energy (eV)
TiO_2–TYS–C/450	137	0.226	3.18
TiO_2–ISOP–C/400	80	0.120	3.04
TiO_2–ISOP–PFC	171	0.265	3.11
TiO_2–ISOP–C/800	0.99	—-	2.90
TiO_2–P25	44	0.208	3.22

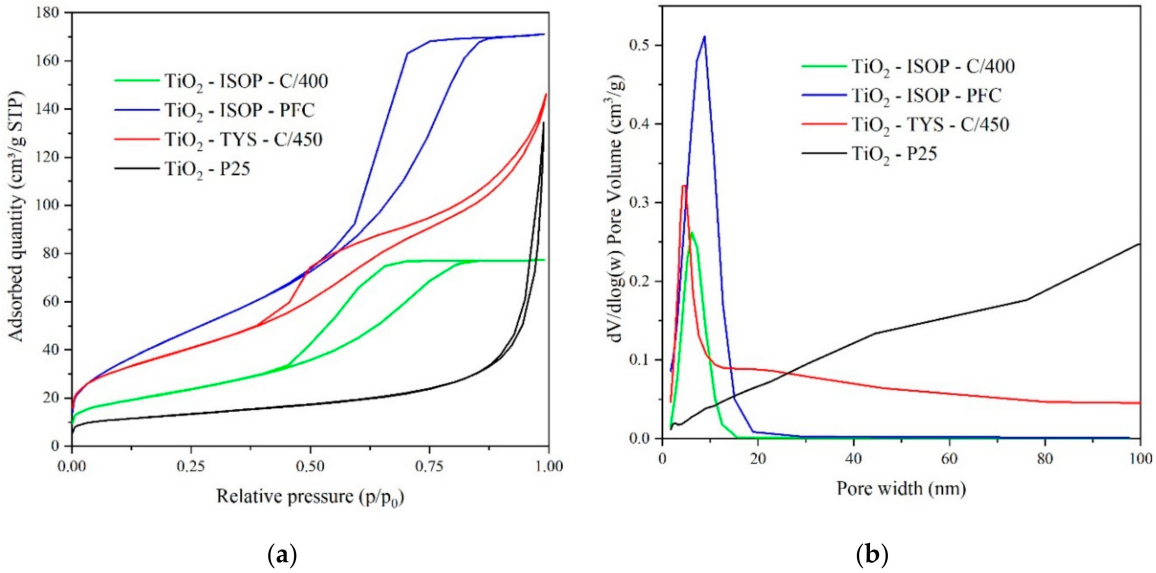

Figure 1. Adsorption/desorption isotherms (**a**) and evaluated pore-size distributions (**b**) of investigated TiO_2 photocatalysts.

In order to evaluate the influence of preparation method of TiO_2 on phase composition, the XRD analysis has been conducted (Figure 2). It is clear the preparation method of TiO_2 significantly influences its phase composition (Table 2). The processing with pressurized hot fluids leads to a formation of bicrystalline phase anatase–brookite, and the calcination results in anatase phase or combination of anatase and rutile, depending on the calcination temperature.

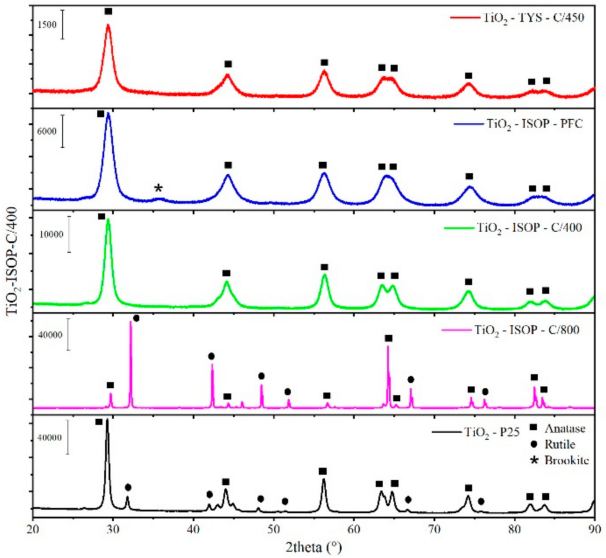

Figure 2. XRD patterns of investigated TiO_2 photocatalysts.

Optical properties were evaluated by UV–vis DRS technique, and the results are shown in Figure 3. The evaluation of band gaps of each photocatalyst was done from Tauc plots after the recalculation of reflectance according to the Kubelka–Munk function (Table 1). The indirect band gaps were evaluated for TiO_2 photocatalysts, therefore, the (K-M·hν) function has to be to power $\frac{1}{2}$ in order to obtain band gap energy. It is clear the preparation method significantly influences the band gap energy of resulting photocatalyst via its phase composition. The lowest band gap energy was 2.90 eV for TiO_2–ISOP–C/800, which contained the highest amount of rutile phase. The largest band gap energy was obtained for the commercial TiO_2–P25 (Evonik).

Table 2. Structural properties of investigated photocatalysts.

Photocatalyst Labeling	Phase Composition (wt.%)	Crystallite-Size (nm)	Facets (hkl)
TiO_2–TYS–C/450	Anatase	7.6	(101) (200)
TiO_2–ISOP–C/400	Anatase	10.3	(101) (200)
TiO_2–ISOP–PFC	79% Anatase	6.5	(101) (200)
	21% Brookite	5.2	(211)
TiO_2–ISOP–C/800	75% Anatase	112	(110) (101) (200)
	25% Rutile	356	(101) (200)
TiO_2–P25	85% Anatase	24	(110) (101) (200)
	15% Rutile	43	(101) (200)

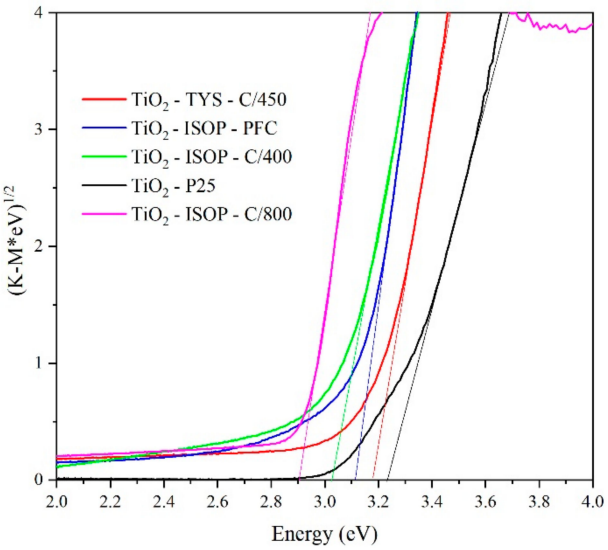

Figure 3. Tauc plots of investigated TiO_2 photocatalysts.

Photocatalysts TiO_2–TYS–C/450 and TiO_2–ISOP–C/400 were prepared by different methods, which leads to different S_{BET} and crystallite-size of anatase (Tables 1 and 2), but their morphology is almost the same (Figure 4). Nevertheless, both photocatalysts contained anatase phase only, and their photocatalytic activity toward removal of organic carbon was comparable. On the other hand, the presence of brookite phase beside anatase led to an increase of TOC removal. The increase in photocatalytic activity can be explained by formation of heterojunction between anatase and brookite phase, as was mentioned earlier [13,14]. TEM image confirmed clusters of very fine particles, which is the benefit of processing by pressurized hot fluids (Figure 4c) [15]. On the other hand, the larger crystallites and through that lower specific surface area was observed at TiO_2–P25 photocatalyst (Figure 4d).

The photocatalytic degradation of MTBE is presented in form of its decreasing concentration over time (Figure 5). MTBE belongs among the volatile organic compounds with a boiling temperature 55.2 °C, therefore time for creating equilibrium between gas and liquid phase is necessary. This is clearly evident from the blank test where the concentration of MTBE decreased during the first 75 min and then stayed more or less constant. Therefore, the 75 min time period was chosen to be sufficient for creating the equilibrium. On the other hand, when pure photolysis was conducted (no photocatalyst present) a significant decrease in MTBE concentration was detected, even after this 75 min dark time. It is clear that the strong UV irradiation itself decomposes the MTBE molecule. The highest decrease of MTBE concentration was observed in the presence of biphasic photocatalysts containing rutile phase (TiO_2–ISOP–C/800 and TiO_2–P25).

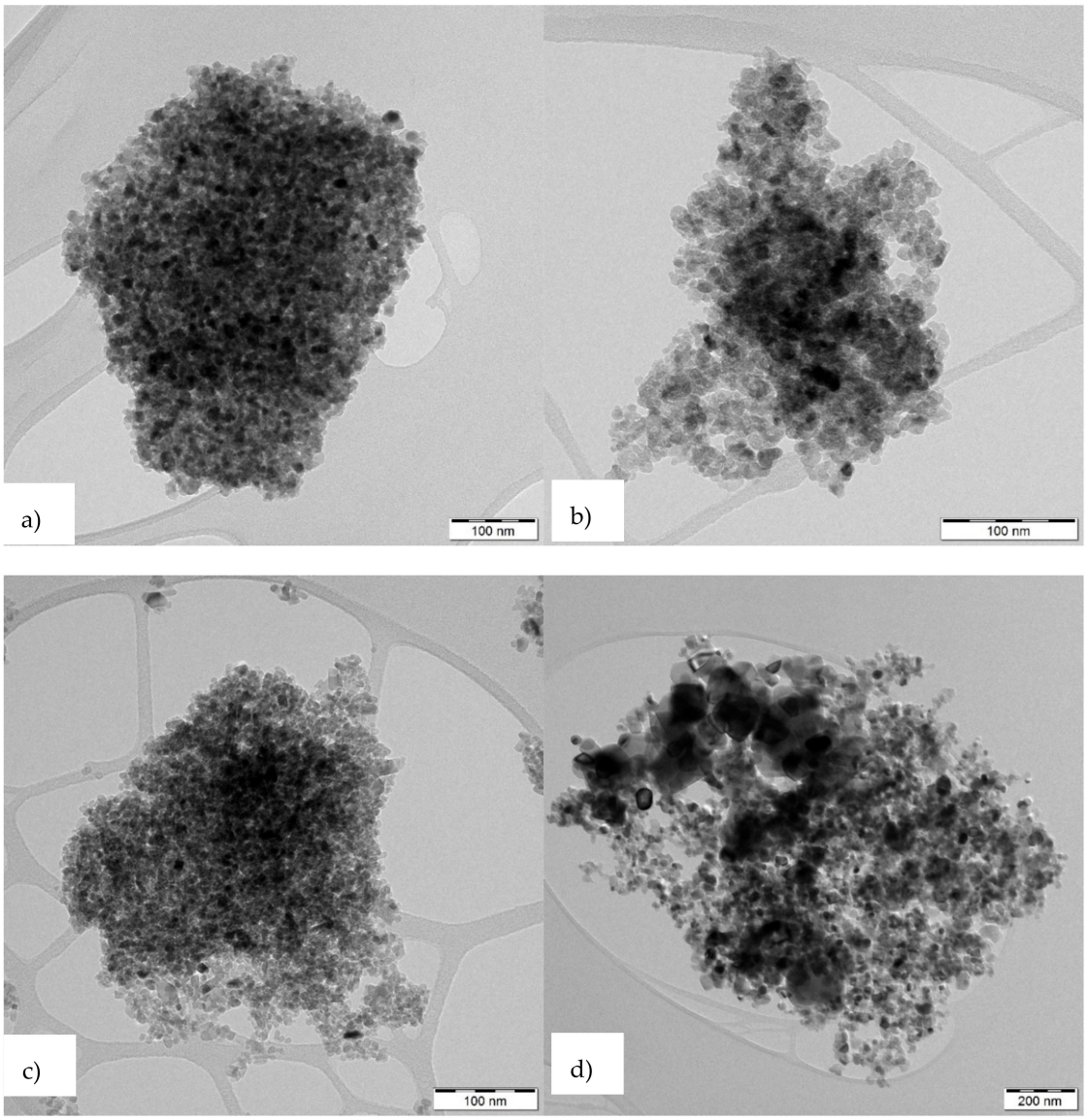

Figure 4. TEM images of (**a**) TiO_2–ISOP–C/400; (**b**) TiO_2–TYS–C/450; (**c**) TiO_2–ISOP–PFC; (**d**) TiO_2–P25.

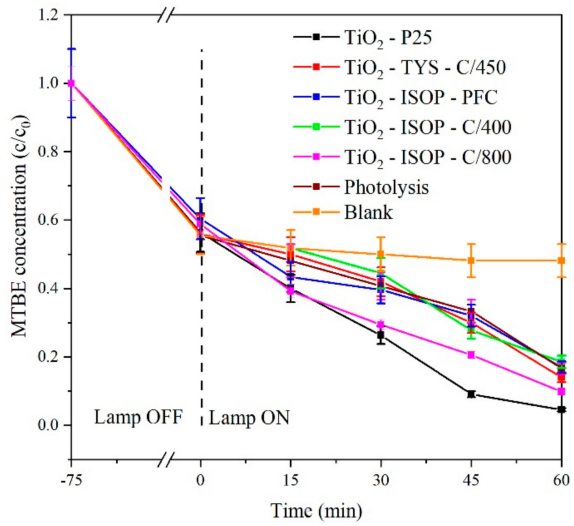

Figure 5. The dependence of MTBE (methyl *tert*-butyl ether) concentration on time over TiO_2 photocatalysts.

The degradation of organic compounds from the waste water is always a tricky one. Since the organic molecule can be oxidized in multiple ways, various by-products, sometimes even more dangerous than the original one, can be produced. There are several by-products reported during the photocatalytic degradation of MTBE, such as formic acid [16], acetaldehyde [16], acetone [17], *tert*-butyl alcohol [16–18], 2-methyl-1-propen [17], *tert*-butyl formate [17], 2-methyl propanoic acid [17], and CO_2 [16,17]. The by-products' production depends on experimental setup and can be different for various research groups.

For the above reasons, it is necessary to monitor not only the decrease of MTBE concentration, but also to analyze the formation of intermediates. Altogether, four different by-products were detected in our case. The presence of each by-product was confirmed by GC/MS and exact concentration in various time was determined the same way as MTBE concentration (SPME method coupled with GC/FID). Figure 6 shows the correlation between the concentration of each by-product and MTBE conversion for individual measurements after 60 min of irradiation. There were four different by-products recognized; acetone (AC), 2-methylprop-1-ene (MP), methyl acetate (MA), and *tert*-butyl formate (TBF). Only 2-methylprop-1-ene was detected in case of blank test, which suggests it is already present in the stock solution of MTBE. The detected by-products were also reported by other groups [17,19]. Since no change in pH was detected during the reaction, we can presume no acidic products, such as formic acid, acetic acid, or propanoic acid, were generated. The main by-product was *tert*-butyl formate. However, the concentration and ratios of by-products' concentrations varied for each photocatalyst, pointing toward the importance in photocatalyst preparation.

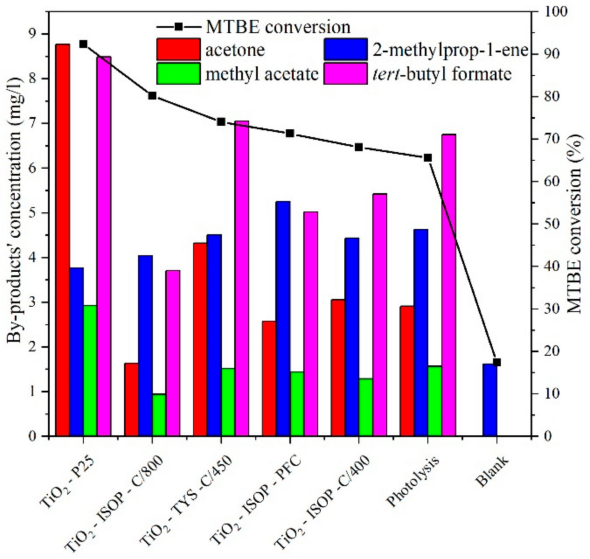

Figure 6. Correlation between by-products' concentrations and MTBE conversion for each photocatalyst, photolysis, and blank measurement after 60 min of irradiation (254 nm).

The formation of by-products in the presence of various photocatalysts is different, which is also evident from Figure 6. In order to compare the photocatalytic activity of each photocatalyst, the amount of total organic carbon (TOC) was calculated and depicted in Figure 7. All prepared photocatalysts performed higher efficiency in TOC removal in comparison with TiO_2–P25. From this point of view, the comparison of two anatase–rutile photocatalysts, i.e., TiO_2–ISOP–C/800 and TiO_2–P25, was very interesting. Even though the removal of MTBE is slightly lower in presence of TiO_2–ISOP–C/800 compared to TiO_2–P25, its photocatalytic activity is higher if we take into account removal of total organic carbon (Figure 7). It suggests that the TiO_2–ISOP–C/800 photocatalyst is more selective toward complete mineralization to CO_2 instead of partial oxidation to organic by-products.

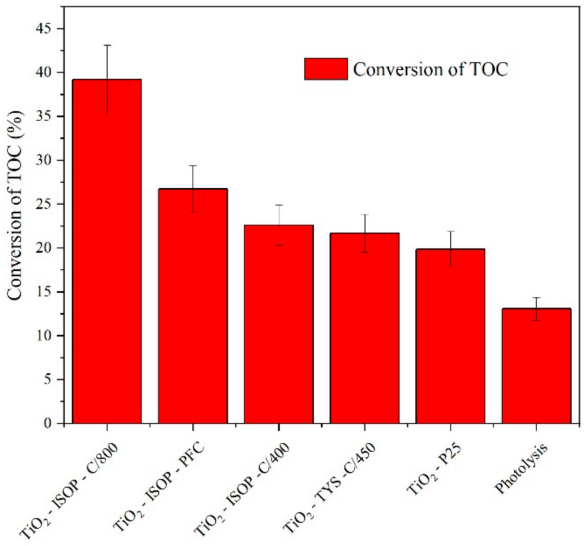

Figure 7. Conversion of total organic carbon (TOC) in presence of each photocatalyst and photolysis after 60 min of irradiation (254 nm).

The photocatalytic activity of photocatalysts depends on many factors such as phase composition, crystallite size, specific surface area, band gap energy, and so on. However, the specific reaction has to be also taken into an account. Prieto-Mahaney et al. [20] studied the correlation between structural and physical properties and photocatalytic activities for five different reactions and 35 TiO_2 samples. They studied six properties, specific surface area, density of lattice defects, primary and secondary particle size, and existence of anatase and rutile phases, to obtain intrinsic dependence of photocatalytic activities on the properties. The role of these properties was significantly depended on the type of photocatalytic reaction. Due to the fact that they did not study photocatalytic decomposition of MTBE, it is not possible compare these results with results obtained in this work. In case of MTBE oxidation, the specific surface area and the crystallite size did not play an important role. The photocatalyst with the highest photoactivity (TiO_2–ISOP–C/800) has the lowest specific surface area and the largest crystallite size. On the basis of the obtained results, we can say that the phase composition was the decisive parameter in the studied reaction. Titanium dioxide has different structures in anatase, rutile, and brookite phase. These differences strongly influence their physicochemical properties.

Our results also confirmed the importance of phase composition of TiO_2. Usually, the presence of two phases leads to a better photocatalytic activity due to the heterojunction between these two phases, which can promote the separation of photogenerated electrons and holes [21]. After absorption of photon, photogenerated electrons can migrate from phase with the higher conduction band (CB) to the phase with lower CB. At the same time, the holes from the phase with a lower valence band (VB) migrate to the phase with a higher VB. For this reason, electrons are separated on one phase of TiO_2 and holes on another one, and both, electrons and holes, can be more efficiently utilized for redox reactions [21,22].

Even though, Figure 6 shows a very slight increase in MTBE conversion in presence of photocatalysts composed solely of anatase or anatase/brookite phase compared to photolysis and photocatalysts containing anatase/rutile proved significantly higher photocatalytic activity toward MTBE oxidation (TiO_2–P25 and TiO_2–ISOP–C/800 removed 95% and 80% of MTBE, respectively), the TOC degradation is the more important factor, which must be considered (Figure 7). Why is the TOC degradation so significant? While TBF can be relatively rapidly degraded as the reaction proceeds, the AC and MA are not only persistent toward radical oxidation, but also a possible oxidation product of TBF [23,24] Due to this reason, the TiO_2–ISOP–C/800 photocatalyst may be considered as the most suitable photocatalyst for degradation of MTBE (Figure 7). This photocatalyst proved not only high conversion of MTBE, but especially the highest conversion of total organic carbon

(the smallest amount of by-products). The TiO_2–P25 showed a very high activity toward removal of MTBE, however, only partial oxidation of organic pollutants was accomplished (Figure 7). In the presence of TiO_2–ISOP–C/800 photocatalyst, the smallest amount of AC (1.64 mg L^{-1}) and MA (0.95 mg L^{-1}) was formed in comparison with TiO_2–P25 (8.77 mg L^{-1} of AC and 2.93 mg L^{-1} of MA). Additionally, another of the bi-phasic photocatalysts (TiO_2–ISOP–PFC), which contained anatase and brookite phase, exhibited good selectivity to the total mineralization. In the presence of TiO_2–ISOP–PFC, 2.58 mg L^{-1} of AC and 1.44 mg L^{-1} of MA were formed. One of the reasons to explain lower photocatalytic activity of TiO_2–P25 toward TOC removal could be a smaller portion of rutile phase in comparison with TiO_2–ISOP–C/800 photocatalyst.

In addition to the formation of heterostructures and the associated reduction in the recombination of electrons and holes, the type of TiO_2 phase is important as well. The rutile phase is more stable, however, usually less photoactive than anatase. It is worth mentioning the charge recombination rate is lower in case of rutile [25]. The most significant difference between the anatase and rutile phases of TiO_2 is in concentration of adsorbed oxygen. The molecular oxygen more easily interacts with oxygen vacancies than with TiO_2 surface, and in addition to that, the interaction is much stronger for rutile than anatase [25]. This fact results in electron transfer from surface defects to an adsorbed oxygen, leading to a formation of superoxide anion (O_2^-). Superoxide anion is a reactive oxygen species, however, its utilization for oxidation of organic compounds is generally low. Nevertheless, $O_2^{\bullet-}$ is an important part in the oxidation process carried out in acidic or neutral environment. It is especially useful in degradation of phenolic compounds, hydroxyl radicals, on the other hand, better oxidize organic intermediates to CO_2 [25]. The above mentioned highlights the necessity of oxygen atmosphere (air) for the oxidation of MTBE. This was confirmed by Barreto et al. [26] who conducted the photocatalytic degradation of MTBE without oxygen as one of the blank tests, and almost no decrease in MTBE concentration was observed.

The adsorbed oxygen molecules reacted with the electron and created superoxide anion radicals (1), which can undergo a few steps, resulting in production of hydrogen peroxide (2) and (3) [16]. The hydrogen peroxide can be reduced by electrons, as well resulting in more hydroxyl radicals and, through that, increasing the conversion of MTBE (4).

$$O_2 + e^- \rightarrow O_2^{\bullet-} \quad (1)$$

$$O_2^{\bullet-} + H^+ \rightarrow HO_2^{\bullet} \quad (2)$$

$$HO_2^{\bullet} + HO_2^{\bullet} \rightarrow H_2O_2 + O_2 \quad (3)$$

$$H_2O_2 + e^- \rightarrow OH^{\bullet} + OH^- \quad (4)$$

$$OH^- + h^+ \rightarrow OH^- \quad (5)$$

Due to this fact, there are two sources of hydroxyl radical-hydrogen peroxide can be produced in the reaction mixture of two-electron transfer (Equation (6)) or water oxidation (Equation (7)) (its formation was found, etc. in [26]).

$$O_2 + 2\,e^- + 2\,H^+ \rightarrow H_2O_2 \quad (6)$$

$$2\,H_2O + 2\,h^+ \rightarrow H_2O_2 + 2\,H^+ \quad (7)$$

For the above reasons, the anatase rutile combination is more effective in oxidizing MTBE than the anatase brookite combination.

Since rutile has significantly higher ability to adsorb oxygen than anatase [25], it is clear why TiO_2–ISOP–C/800 sample has higher photocatalytic activity toward TOC conversion than all the other photocatalysts. There is the highest amount of rutile present and therefore, there is the highest

separation of charge carriers, either through heterojunction or by easier reduction of adsorbed oxygen to superoxide anion radical.

Reaction Mechanism

Mohebali et al. [17] proposed two reaction path ways leading to either 2-methyl propanoic acid or acetic acid. The important thing to know is what initiates the oxidation of organic molecule; is it photogenerated hole itself or hydroxyl radical created from the water oxidation? It is well known electron–hole pair is generated after absorption of photon with sufficient energy by TiO_2 (1). In order to find out whether the reaction is initiated by hole or hydroxyl radical experiment with isopropyl alcohol was carried out (see Supplementary Materials). Isopropyl alcohol serves as hydroxyl radical scavenger, therefore, the reaction rate would decrease if hydroxyl radicals oxidize MTBE and stayed the same in case holes oxidize MTBE molecule [27]. The test was carried out repeatedly in presence of TiO_2–P25. Since the conversion of MTBE decreased from 92% (without isopropanol) to 37% (with 0.19 mL isopropanol) we can safely assume the oxidation of MTBE is initiated by hydroxyl radicals created from single hole water oxidation (2). These findings are in an agreement with Hwang et al. [27]. The most represented by-product, *tert*-butyl formate (TBF), is formed through two steps according (3).

The reduction of adsorbed oxygen by photogenerated electron helps to charge carriers' separation and lowers the recombination rate. Therefore, another experiment was conducted. This time, chloroform as superoxide anion radical scavenger was added (see Supplementary Materials). Chloroform willingly interacts with superoxide anion radicals shifting the equilibrium so more superoxide anion radicals are produced and the separation of charge carriers is even more enhanced. This was confirmed experimentally where the addition of chloroform (0.016 mL) increased the MTBE conversion to 100% from 92% in presence of TiO_2–P25.

3. Materials and Methods

3.1. Photocatalysts Preparation Method

Altogether, 4 different TiO_2 photocatalysts were prepared, using either titanyl sulphate or titanium (IV) isopropoxide as Ti-precursor depending on the used chemical method (thermal hydrolysis vs. sol-gel), and different processing (pressurized hot solvents crystallization vs. calcination). The preparation method and processing for individual TiO_2 photocatalysts is described in Table 3.

Table 3. Information about preparation of investigated TiO_2 photocatalysts.

Photocatalysts Labeling	Preparation		Processing	
	Method	Precursor	Method	Conditions
TiO_2–TYS–C/450	Thermal hydrolysis	Titanyl sulphate	Calcination	450 °C (2 h), 3 °C min^{-1}
TiO_2–ISOP–C/400	Sol-gel	Titanium (IV) isopropoxide	Calcination	400 °C (4 h), 10 °C min^{-1}
TiO_2–ISOP–PFC	Sol-gel	Titanium (IV) isopropoxide	Pressurized hot fluids crystallization	200 °C, 10 MPa, 1.5 L H_2O + 0.25 L CH_3OH + 0.1 L H_2O, 3.5–4.5 mL min^{-1}
TiO_2–ISOP–C/800	Sol-gel	Titanium (IV) isopropoxide	Calcination	800 °C (4 h), 5 °C min^{-1}

The preparations of individual TiO_2 were following:

TiO_2–TYS–C/450: The titanium precursor stock solution was prepared from titanyl sulphate monohydrate ($TiOSO_4$ H_2O). The solution was stirred with a spindle stirrer for 3 days until complete dissolution of titanyl sulphate monohydrate in water. The final concentration of stock solution was 100 g of TiO_2 L^{-1} of solution. Then the stock solution was mixed with 0.5 wt.% H_2SO_4 solution and stirred at temperature of 80 °C on a magnetic stirrer for 60 min. The solution was cooled at laboratory

temperature. After cooling, a 20 wt.% NaOH solution was added until the pH of the solution rose to 7. The resulting suspension was filtered using a Buchner funnel. The collected precipitate was washed with demineralized water until the sulfates were removed. The presence of sulfates was verified using $BaCl_2$ solution. The obtained precipitate was dried in an oven at 50 °C for 24 h to constant weight. Afterwards, the precipitate was calcined in an oven at 450 °C for 2 h using a temperature ramp of 3 °C min^{-1}.

TiO_2–ISOP–C/400: Titania sol was prepared by mixing cyclohexane, Triton X-114, demineralized water, and titanium (IV) isopropoxide in molar ratio of 11:1:1:1. Firstly, cyclohexane, Triton X-114, and water were mixed and stirred for 15 min. Then titanium (IV) isopropoxide was added and the micellar sol was mixed for 30 min for homogenization. Afterwards, the sol was poured into a Petri dish and aged for 48 h on air. The gelation of sol took place. The gel was crashed to 3 × 3 mm small pieces, placed in crucibles, and calcined in an oven at 400 °C for 4 h using a temperature ramp of 10 °C min^{-1} to obtain TiO_2 powder. The powder sample was sieved to particle size < 0.160 mm.

TiO_2–ISOP–PFC: The titanium-based gel was prepared identically as mentioned in the case of TiO_2–ISOP–C/400, but the crashed gel was crystallized at 200 °C and 10 MPa, using the sequence of solvents: 1.5 L of demineralized water, 0.25 L of methanol, and 0.1 L of demineralized water with a flow rate of 3.5–4.5 mL min^{-1} to obtain TiO_2 powder. The powder sample was sieved to particle size < 0.160 mm.

TiO_2–ISOP–C/800: The titanium-based gel was prepared identically as mentioned in the case of TiO_2–ISOP–C/400, but the crashed gel was calcined in an oven at 800 °C for 4 h using a temperature ramp of 5 °C min^{-1} to obtain TiO_2 powder. The powder sample was sieved to particle size < 0.160 mm.

TiO_2–P25: Commercially available TiO_2 powder (particle size < 0.09 mm) used as a reference photocatalyst to be compared with investigated prepared photocatalysts.

3.2. Characterization of TiO_2 Photocatalysts

Each photocatalyst was characterized by several characterization techniques, such as nitrogen physisorption [28], powder X-ray diffraction [29], transmission electron microscopy [28], and diffuse reflectance UV-vis spectroscopy [30]. For more detail see Supplementary Materials.

3.3. Photocatalytic Degradation of MTBE

The annular batch photoreactor was used for the photocatalytic degradation of MTBE. The photoreactor was homemade from stainless steel and was fitted with stoppers around its inner periphery in order to achieve better mixing. Total volume of the photoreactor was 305 mL. The suspension of 0.1 g of photocatalyst in the 100 mL MTBE solution was used for the photocatalytic test. The concentration of MTBE was 70 μmol L^{-1} (52 mg L^{-1}). The mixture was stirred using magnetic stirrer at 600 rpm. The reactor was sealed in order to monitor composition of the gas phase, which was air at the beginning of the reaction. The gas sample was taken at 0 h and analyzed on GC/BID. The solution was left in the dark for 75 min in order to reach adsorption/desorption equilibrium. Reaction itself started by turning on the 8 W Hg lamp with peak intensity at 254 nm, which was placed in quartz glass tube in the axis of symmetry of the reactor. The photocatalytic test was carried out for 60 min, and samples were taken each 15 min. Liquid samples (2 mL) were taken through septum at the bottom of the reactor, and the photocatalyst was filtered out using syringe filters with quartz pre-filter. The composition of the liquid phase was analyzed using SPME method (Solid Phase Micro Extraction) and GC/FID.

4. Conclusions

MTBE represents a rising threat to the environment and its effective removal (with all the by-products) is necessary. This work investigates MTBE oxidation in presence of various TiO_2 photocatalysts prepared by different methods. The TiO_2–ISOP–C/800 photocatalyst showed significantly higher activity toward TOC removal and also high activity for MTBE conversion. Base on the results the phase composition of TiO_2 was found to be the key parameter in the photocatalytic degradation of

MTBE. Notably, the presence of the heterojunction in biphasic TiO_2 photocatalysts is profitable, because it enables better separation of electrons and holes. Furthermore, the rutile phase, unlike brookite phase, more easily reduce adsorbed oxygen by photogenerated electrons to superoxide radical, which also supports the separation of charge carriers leading to higher photocatalytic activity.

Supplementary Materials: The following are available online at http://www.mdpi.com/2073-4344/10/1/35/s1, Figure S1: Dependence of MTBE conversion on time in presence of TiO_2 P25 without and with scavengers of $OH^{\bullet}$ and $O_2^{\bullet-}$.

Author Contributions: Photocatalytic measurements, M.Š.; preparation of analytical method, K.H.; photocatalysts preparation, M.V. and L.M.; Writing—Original draft preparation, M.R.; Writing—Review and editing, K.K. and M.R. All authors have read and agreed to the published version of the manuscript.

Funding: This research was funded by EU structural funding in Operational Programme Research Development and Education "IET-ER", grant number CZ.02.1.01/0.0/0.0/16_019/0000853, by Ministry of Industry and Trade, grant number CZ.01.1.02/0.0/0.0/16_084/0010305 and Large Research Infrastructure "ENREGAT" supported by the Ministry of Education, Youth and Sports of the Czech Republic, grant number LM2018098.

Conflicts of Interest: The authors declare no conflict of interest.

References

1. Levchuk, I.; Bhatnagar, A.; Sillanpää, M. Overview of technologies for removal of methyl *tert*-butyl ether (MTBE) from water. *Sci. Total Environ.* **2014**, *476*, 415–433. [CrossRef] [PubMed]
2. U.S. Environmental Protection Agency (EPA). Methyl Tertiary Butyl Ether (MTBE)—Overview. Available online: https://archive.epa.gov/mtbe/web/html/faq.html (accessed on 16 October 2018).
3. Media, A. *Argus MTBE Annual 2017*; Argus Media: London, UK, 2017; pp. 1–6.
4. Park, S.E.; Joo, H.; Kang, J.W. Photodegradation of methyl tertiary butyl ether (MTBE) vapor with immobilized titanium dioxide. *Sol. Energy Mater. Sol. Cells* **2003**, *80*, 73–84. [CrossRef]
5. Zang, Y.; Farnood, R. Photocatalytic decomposition of methyl *tert*-butyl ether in aqueous slurry of titanium dioxide. *Appl. Catal. B* **2005**, *57*, 275–282. [CrossRef]
6. Orlov, A.; Jefferson, D.A.; Tikhov, M.; Lambert, R.M. Enhancement of MTBE photocatalytic degradation by modification of TiO_2 with gold nanoparticles. *Catal. Commun.* **2007**, *8*, 821–824. [CrossRef]
7. Rodríguez-González, V.; Zanella, R.; Del Angel, G.; Gómez, R. MTBE visible-light photocatalytic decomposition over Au/TiO_2 and Au/TiO_2–Al_2O_3 sol–gel prepared catalysts. *J. Mol. Catal. A Chem.* **2008**, *281*, 93–98. [CrossRef]
8. Mirhoseini, F.; Salabat, A. Removal of methyl *tert*-butyl ether as a water pollutant by photodegradation over a new type of poly(methyl methacrylate)/TiO_2 nanocomposite. *Polym. Compos.* **2018**, *39*, 1248–1254. [CrossRef]
9. Seddigi, Z.S.; Ahmed, S.A.; Bumajdad, A.; Danish, E.Y.; Shawky, A.M.; Gondal, M.A.; Soylak, M. The efficient photocatalytic degradation of methyl *tert*-butyl ether under Pd/ZnO and visible light irradiation. *Photochem. Photobiol.* **2015**, *91*, 265–271. [CrossRef] [PubMed]
10. Seddigi, Z.S.; Ahmed, S.A.; Bumajdad, A.; Gonadal, M.A.; Danish, E.Y.; Shawky, A.M.; Yarkandi, N.H. Photocatalytic degradation oftert-butyl alcohol andtert-butyl formate using palladium-doped zinc oxide nanoparticles with UV irradiation. *Desalin. Water Treat.* **2015**, 1–10. [CrossRef]
11. Klauson, D.; Gromyko, I.; Dedova, T.; Pronina, N.; Krichevskaya, M.; Budarnaja, O.; Oja Acik, I.; Volobujeva, O.; Sildos, I.; Utt, K. Study on photocatalytic activity of ZnO nanoneedles, nanorods, pyramids and hierarchical structures obtained by spray pyrolysis method. *Mater. Sci. Semicond. Process.* **2015**, *31*, 315–324. [CrossRef]
12. Sing, K.S.W.; Everett, D.H.; Haul, R.A.W.; Moscou, L.; Pierotti, R.A.; Rouquerol, J.; Siemieniewska, T. Reporting Physisorption Data for Gas/Solid Systems. *Pure Appl. Chem.* **1985**, *57*, 603–619. [CrossRef]
13. Reli, M.; Kobielusz, M.; Matějová, L.; Daniš, S.; Macyk, W.; Obalová, L.; Kuśtrowski, P.; Rokicińska, A.; Kočí, K. TiO_2 Processed by pressurized hot solvents as a novel photocatalyst for photocatalytic reduction of carbon dioxide. *Appl. Surf. Sci.* **2017**, *391*, 282–287. [CrossRef]
14. Matějová, L.; Šihor, M.; Lang, J.; Troppová, I.; Ambrožová, N.; Reli, M.; Brunátová, T.; Čapek, L.; Kotarba, A.; Kočí, K. Investigation of low Ce amount doped-TiO_2 prepared by using pressurized fluids in photocatalytic N_2O decomposition and CO_2 reduction. *J. Sol-Gel Sci. Technol.* **2017**, *84*, 158–168. [CrossRef]
15. Matějová, L.; Matěj, Z.; Fajgar, R.; Cajthaml, T.; Šolcová, O. TiO_2 powders synthesized by pressurized fluid extraction and supercritical drying: Effect of water and methanol on structural properties and purity. *Mater. Res. Bull.* **2012**, *47*, 3573–3579. [CrossRef]

16. Araña, J.; Peña Alonso, A.; Doña Rodríguez, J.M.; Herrera Melián, J.A.; González Díaz, O.; Pérez Peña, J. Comparative study of MTBE photocatalytic degradation with TiO_2 and Cu-TiO_2. *Appl. Catal. B* **2008**, *78*, 355–363. [CrossRef]
17. Mohebali, S. Degradation of methyl *t*-butyl ether (MTBE) by photochemical process in nanocrystalline TiO_2 slurry: Mechanism, by-products and carbonate ion effect. *J. Environ. Chem. Eng.* **2013**, *1*, 1070–1078. [CrossRef]
18. Hu, Q.; Zhang, C.; Wang, Z.; Chen, Y.; Mao, K.; Zhang, X.; Xiong, Y.; Zhu, M. Photodegradation of methyl *tert*-butyl ether (MTBE) by UV/H_2O_2 and UV/TiO_2. *J. Hazard. Mater.* **2008**, *154*, 795–803. [CrossRef]
19. Selli, E.; Letizia Bianchi, C.; Pirola, C.; Bertelli, M. Degradation of methyl *tert*-butyl ether in water: Effects of the combined use of sonolysis and photocatalysis. *Ultrason. Sonochem.* **2005**, *12*, 395–400. [CrossRef]
20. Prieto-Mahaney, O.-O.; Murakami, N.; Abe, R.; Ohtani, B. Correlation between Photocatalytic Activities and Structural and Physical Properties of Titanium(IV) Oxide Powders. *Chem. Lett.* **2009**, *38*, 238–239. [CrossRef]
21. Bai, S.; Jiang, J.; Zhang, Q.; Xiong, Y. Steering charge kinetics in photocatalysis: Intersection of materials syntheses, characterization techniques and theoretical simulations. *Chem. Soc. Rev.* **2015**, *44*, 2893–2939. [CrossRef]
22. Zhang, Y.; Gan, H.; Zhang, G. A novel mixed-phase TiO_2/kaolinite composites and their photocatalytic activity for degradation of organic contaminants. *Chem. Eng. J.* **2011**, *172*, 936–943. [CrossRef]
23. Huang, K.C.; Couttenye, R.A.; Hoag, G.E. Kinetics of heat-assisted persulfate oxidation of methyl *tert*-butyl ether (MTBE). *Chemosphere* **2002**, *49*, 413–420. [CrossRef]
24. Hetflejš, J.; Šabata, S.; Kuncová, G. *terc*-butylmethylether a jeho degradace oxidačními procesy. *Chem. Listy* **2007**, *101*, 1011–1019.
25. Buchalska, M.; Kobielusz, M.; Matuszek, A.; Pacia, M.; Wojtyla, S.; Macyk, W. On Oxygen Activation at Rutile- and Anatase-TiO_2. *ACS Catal.* **2015**, *5*, 7424–7431. [CrossRef]
26. Barreto, R.D.; Gray, K.A.; Anders, K. Photocatalytic degradation of methyl-*tert*-butyl ether in TiO_2 slurries: A proposed reaction scheme. *Water Res.* **1995**, *29*, 1243–1248. [CrossRef]
27. Hwang, S.; Huling, S.G.; Ko, S. Fenton-like degradation of MTBE: Effects of iron counter anion and radical scavengers. *Chemosphere* **2010**, *78*, 563–568. [CrossRef]
28. Troppová, I.; Šihor, M.; Reli, M.; Ritz, M.; Praus, P.; Kočí, K. Unconventionally prepared TiO_2/g-C_3N_4 photocatalysts for photocatalytic decomposition of nitrous oxide. *Appl. Surf. Sci.* **2018**, *430*, 335–347. [CrossRef]
29. Reli, M.; Troppová, I.; Šihor, M.; Pavlovský, J.; Praus, P.; Kočí, K. Photocatalytic decomposition of N_2O over g-C_3N_4/$BiVO_4$ composite. *Appl. Surf. Sci.* **2019**, *469*, 181–191. [CrossRef]
30. Reli, M.; Svoboda, L.; Šihor, M.; Troppová, I.; Pavlovský, J.; Praus, P.; Kočí, K. Photocatalytic decomposition of N_2O over g-C_3N_4/WO_3 photocatalysts. *Environ. Sci. Pollut. Res. Int.* **2017**, 1–12. [CrossRef]